CrossMark

TECHNICAL PAPER

Design and simulation of pyroelectric detectors with nanometer size spider-web for low thermal conductance

Md A. Muztoba[1] · Noureddine Melikechi[2] · Mukti M. Rana[2]

Abstract We report the design and simulation of uncooled pyroelectric detectors which utilizes a nanometer sized mesh or truss to support the suspended detector. Pyroelectric detector is a class of thermal detector in which the change in temperature causes the change in the spontaneous polarization in the sensing material. Ca modified lead titanate (PCT) was selected as the thermometer in the detector because of its high pyroelectric figure of merit. The design and simulation of pyroelectric detectors have been conducted by simulating the structure with Intellisuite™. Finite element method (FEM) was used to simulate the structural and thermal properties of the device. The simulated detectors had a spider web-like structure with each of the strut (ring) of spider web had a width of 100 nm. In the design, the pyroelectric detectors utilized $Ni_{0.8}Cr_{0.2}$ absorber, PCT sensing layer, Ti electrodes, Al_2O_3 structural layer to obtain low thermal conductance between the detector and Si substrate. Three different types of pyroelectric detectors were designed and analyzed. The first design had linear electrode and simple spider web support. The value of the thermal conductance of this detector was found to be 3.98×10^{-8} W/K. The second design had a longer thermal path than the first one and the thermal conductivity of this device was found to be 2.41×10^{-8} W/K. High detectivity was obtained by reducing the thermal conductance between the sensing layer and the substrate or the heat sink in the

third design. The design was optimized for the best result by modifying the shape, dimension and thickness of various layers namely absorber, electrodes, sensing layer, and struts. The thermal conductance between the sensor and the substrate using the third design was found to be as low as 4.57×10^{-9} W/K which is significantly lower than previously reported values. The thicknesses of the web structure, web support, electrodes, sensing layer, and absorber of the final structure were 2, 1, 0.5, 2, and 0.2 μm respectively for this value of thermal conductance. The absorber diameter was 50 μm and the diameter of the spider web was 200 μm. A total of 80 struts with 100 nm width were used in the design.

1 Introduction

Pyroelectric detectors are a class of thermal infrared (IR) detector in which a change in temperature causes a change in the spontaneous polarization of the sensing material. Since a pyroelectric detector does not require any bias current to operate, it is free of $1/f$-noise. Thermal IR detectors can operate at room temperature which is a major advantage compared to photon detectors. Background limited cryogenic detectors have been designed in the past for operation in the long wave region of 8–14 μm, although these types of detectors cannot operate at room temperature.

Uncooled infrared detectors are ideally suited for many IR applications in both commercial and military sectors. They are used in surveillance (Parker et al. 1996; Flannery and Milelr 1992), firefighting (Rogalski 2003; Mehta et al. 2005), medical monitoring (Rogalski 2003), military (Flannery and Milelr 1992), automotive night vision (Niklaus 2007) and scientific instruments such as spectrometers (Rajendra Kumara et al. 2003) and radiometers (Kruse

✉ Mukti M. Rana
mrana@desu.edu

[1] Department of Electrical Engineering, Arizona State University, P.O. Box 9309, Tempe, AZ 85287-9309, USA

[2] Department of Physics and Engineering and Optical Science Center for Applied Research (OSCAR), Delaware State University, Dover, DE 19901, USA

🖄 Springer

1997). They provide good performance that has enabled systems to be developed which have reduced size, weight, and power consumption. Yet uncooled IR detectors still have not reached their fundamental limits of performance. The evolution of electron-beam lithography, nanoimprinting, and deep ultraviolet lithography has enabled sub-100 nm features to be patterned.

By utilizing nano-lithography, the design aspects of uncooled pyroelectric detectors with low thermal conductance have been investigated in this report. Here, in this design and simulation work, we used a nanometer sized mesh or truss to support the micromachined detector, thereby providing a thermal conductance that is limited by the radiative heat exchange with the environment. Ca-modified lead titanate has a high pyroelectric figure of merit and was employed as the thermometer in the detector. Intellisuite™, a commercially available engineering design software, was used to simulate the structural and thermal properties of the device. Three different types of pyroelectric detectors were designed and analyzed. For each design the effects of thickness, dimension and width of each layer were studied. Mathcad Engineering calculation software was used to analyze the performance.

2 Background

Pyroelectricity is the electrical response of a polar, dielectric material to a change in temperature. This property is present in certain materials that exhibit a change in electric polarization Δp, when a temperature variation ΔT is applied uniformly and is related by the following relation:

$$\Delta p = \gamma \Delta T \tag{1}$$

where, γ is the pyroelectric coefficient at constant stress and can be expressed as:

$$\gamma = \frac{\partial P_S}{\partial T} \tag{2}$$

where, P_s is the spontaneous polarization.

Spontaneous polarization changes when the detector is heated by any electromagnetic radiation caused by the heat flux. When the surface temperature is changed, the surface charges redistribute among themselves which can be measured between conductive electrodes of the substance. This effect is called pyroelectric effect (Kao 2004).

Pyroelectric detector is a planar capacitor whose charge Q varies according to

$$\Delta Q = A\gamma \Delta T \tag{3}$$

where, A is the area of the capacitor.

The detector can be represented by a thermal capacitance C_{th} coupled via a thermal conductance G_{th} to a heat sink which is maintained at a constant temperature T. The rise in temperature due to a modulating heat flux is found by solving the heat balance equation described below

$$\Delta T = \frac{\eta \phi}{G_{eff} \sqrt{1 + \omega^2 \tau_{th}^2}} \tag{4}$$

where, ΔT is the temperature difference between the detector and its surroundings i.e., T due to periodic heat flux Φ, η is the average absorption coefficient of the detector and G_{eff} is the effective thermal conductance given by,

$$G_{eff} = G_{rad} + G_{th} \pm \alpha P_{bias} \tag{5}$$

where, α is the TCR of the thermometer and P_{bias} is the power dissipated because of the bias current of the detector. This term can be cancelled for pyroelectric detectors since they can operate without bias.

Radiative thermal conductance, G_{rad}, is the radiative thermal conductance for a gray body, assuming the emissivity is equal to the absorptivity, is given by $4\eta\sigma AT^3$ where σ is the Stefan-Boltzmann constant, A is the surface area, and T is the absolute temperature. As far as the design is concern, not much can be done other than material selection to reduce G_{rad}. However, the materials known for low heat loss also absorbs less infrared radiation, which is undesirable. This put the ultimate limit on the performance of the detector. G_{rad} can dominate for detectors with low thermal conductance, G_{th}, and bias heating should be avoided.

There are two possible ways for thermal conduction G_{th}. First, the heat is lost through conduction/convection through the atmosphere surrounding the detector thermometer which can be minimized by vacuum packaging the detector. Second, the heat is lost by thermal conduction through the supporting structure of the thermometer. The design of the supporting structure directly impacts the thermal conductance.

Equation (3) indicates that a larger ΔT will lead to a larger ΔQ which means a better detection of radiation. However Eq. (4) shows that G_{eff} must be low for larger ΔT. From Eq. (5) we can see that for pyroelectric detectors, the effective thermal conductance is due to mainly thermal conduction through the supporting structure of the thermometer. So, the thermal conductivity between the heat sink and thermometer must be made as small as possible to obtain a lower value of thermal conductance. In this work, the aim was set toward achieving a greater ΔT by ensuring lower thermal conductance through the supporting structures.

2.1 Simulated device description and the design parameters

Efficient absorber design with very low thermal conductance to the substrate is necessary to obtain a high
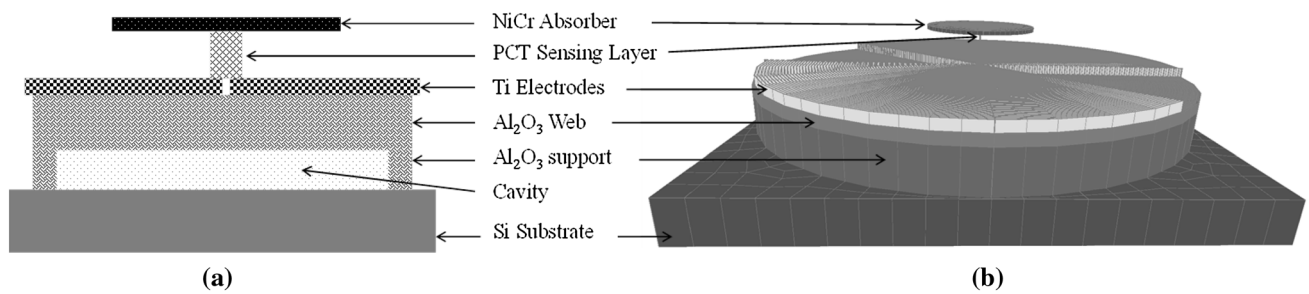
Fig. 1 Geometry of the final structure of detector, **a** Cross sectional view, **b** 3-D view generated by FEM Software Intellisuite™

Table 1 Thermal conductance of detectors found by calculations based on FEM

Device	Description	Thermal conductance (W/K)
1	Simple circular spider web with linear electrodes	3.98×10^{-8}
2	Meandered circular spider web with linear electrodes	2.41×10^{-8}
3	Meandered circular spider web with meander electrodes	4.57×10^{-9}

detectivity. An important part of all IR detector systems is the absorber efficiency that indicates how much heat falling on the surface of the detector is converted into transduced signal. A circular $Ni_{0.8}Cr_{0.2}$ absorber was used for the design as $Ni_{0.8}Cr_{0.2}$ has high absorption at infrared frequencies. Si was used as the substrate because of its excellent electrical and mechanical properties. Ti was selected as the electrode material since it has relatively lower thermal conductivity along with high electrical conductivity.

Spider web superconducting microbolometers have been demonstrated by utilizing a Si_3N_4 spider web like pattern to suspend the thermometer (Gildemeister et al. 2007; Kiewiet et al. 1999). A low thermal conductance of 1×10^{-10} W/K was achieved from that structure at cryogenic temperature. However, the area of the spider web pattern was 3.5 mm in diameter for the 7 μm wide Si_3N_4 struts in the spider web (Gildemeister et al. 2007). The thermal conductance was further reduced to 3.2×10^{-11} W/K with an area of 1.4 mm in diameter for the 5 μm wide struts. To achieve an uncooled infrared detector with a radiation limited thermal conductance, the thermal conductance needs to be $\sim 5 \times 10^{-9}$ W/K. By utilizing a struss-like mesh, the supporting structure maintained mechanical strength as with the spider web pattern and similarly had a low thermal conductance. In this work, Al_2O_3 is utilized as the structural material of the micromachined detectors. Al_2O_3 offers some structural advantages over Si_3N_4 in that it possesses higher yield strength of 15.4 GPa (http://memsnet.org/material/. Accessed 1 Nov 2012) compared with 8.7 GPa for Si_3N_4 (Qian et al. 2005).

Lead Titanate is known to have good piezo, pyro and ferroelectric properties. However, it has poor mechanical properties due to its large tetragonal ratio. Hence, several modifications of this material have been studied with the aim of obtaining improved electrical and mechanical

properties to make them potentially useful for various applications. Calcium modified lead titanate has received some attention because of its better mechanical stability and enhanced sensing properties (Seifert et al. 1998). It has been shown to have a high pyroelectric figure of merit and is considered to be a very good candidate for thin film pyroelectric detector (Chopra et al. 2004; Chang and Lai 2007). A 30 % Ca content was found to deliver the best pyroelectric detector behavior (Chang and Lai 2007). The addition of Ca decreased the dielectric constant while maintaining relatively the same pyroelectric constant thereby increasing the Johnson noise limited detectivity figure of merit as seen from the following expression,

$$D^* = \frac{\eta d}{\sqrt{4kT}} \frac{1}{\sqrt{\omega}} \frac{p}{c'\sqrt{\varepsilon_r \varepsilon_0 \tan \delta}} \qquad (6)$$

So, PCT was selected as sensor material for infrared radiation sensing.

The geometry of the device used for the device simulation and design is shown in Fig. 1 while Table 1 shows the values of constant used for device design by utilizing IntelliSuite™.

The fabrication process of the devices was simulated in InlelliSuite™. IntelliMask™ and Blueprint™ were used for constructing all device level masks. The materials were imported from the thin-film material database MEMaterial® and properties mentioned in Table 2 were used. Thermal conductivity, density and young modulus of PCT were assumed to be same as that of PZT. Also, the Poisson ratio of PCT was assumed to be 0.25 since this parameter had negligible effect on the result. The virtual fabrications were done in process simulation module IntelliFAB™ of InlelliSuite™ Engineering Design Software. The fabricated model is shown in Fig. 2.

Table 2 Thermal and mechanical properties of materials used for simulation and design of pyroelectric detector

Material	Si	Al_2O_3	Ti	PCT	$Ni_{0.8}Cr_{0.2}$
Thermal conductivity (W/m/K)	150 (Glassbrenner and Slack 1964)	25 (Mahmood 2006)	21.9 (http://memsnet.org/material/)	1.3 (Kallaeva et al. 2006)	90 (http://memsnet.org/material/)
Specific heat (J/kg/K)	702.24 (http://memsnet.org/material/)	770 (http://memsnet.org/material/)	522.5 (http://memsnet.org/material/)	303 (Rossetti et al. 2005)	443.9 (http://memsnet.org/material/)
Density (kg/m3)	2330 (http://memsnet.org/material/)	4000 (http://memsnet.org/material/)	4510 (http://memsnet.org/material/)	7500 (http://memsnet.org/material/)	8566 (http://memsnet.org/material/)
Young modulus (GPa)	165 (http://memsnet.org/material/)	350 (http://memsnet.org/material/)	110 (http://memsnet.org/material/)	10,000 (http://memsnet.org/material/)	188 (http://memsnet.org/material/)
Poisson ratio	0.22 (http://memsnet.org/material/)	0.24 (http://memsnet.org/material/)	0.33 (Mahmood 2006)	0.25	0.29 (James and Lord 1992)
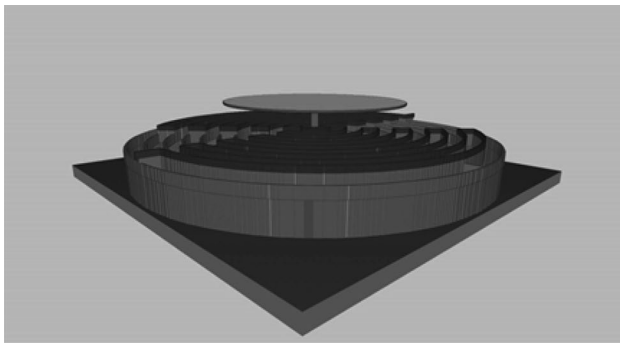
Fig. 2 Virtually fabricated pyroelectric detector using FEM Software Intellisuite™

3 Results from the simulations and discussions

Three types of pyroelectric detectors were designed and analyzed. The difference among the designs was in the shape of the spider web support and electrodes as shown in Fig. 3. For each design the effects of thickness, dimension and width of each layer were studied as shown in Fig. 4.

Thermal conductance of the structure was calculated from,

$$G_{th} = \frac{A}{\Delta T} I \tag{7}$$

where, A is the area of the absorber and I is the intensity of the heat flux. The temperature rise for heat conduction process is related to the path length as,

$$\Delta T = \frac{L}{G_{th}} I \tag{8}$$

where L is the thermal path length. The temperature rise is directly proportional to the thermal path length and therefore a lower thermal conductance was obtained by making the path length longer.

Device 1 had simple circular spider web supporting structure and lined electrodes (see Fig. 3a). It was found that the junctions between each rings of the supporting structure were responsible for transferring most of the heat away to the substrate. So for device 2, the web structure was meandered (see Fig. 3b) to achieve a longer thermal path which provided a lower thermal conductance than device 1. Still, the linear electrodes were acting like means of direct conduction of heat from the center to the periphery of the device. So the electrodes were also meandered

Fig. 3 Top view of the spider web support and electrodes for three designs, **a** device 1: simple circular spider web with linear electrodes, **b** device 2: meandered circular spider web with linear electrodes, and **c** device 3: meandered circular spider web with meander electrodes
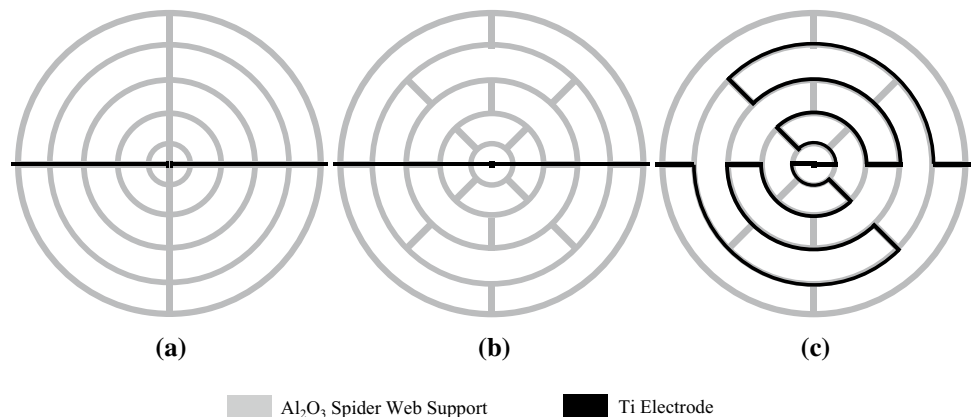

(a) **(b)** **(c)**

▨ Al_2O_3 Spider Web Support ■ Ti Electrode

Fig. 4 Study of effects of **a** dimension of absorber, **b** dimension of web, **c** number of struts, **d** thickness of absorber, **e** thickness of electrode, **f** thickness of sensinglayer, **g** thickness of web structure, **h** thickness of web support, and **i** width of struts on thermal conductance on the device performance determined by simulation done by Intellisuite™
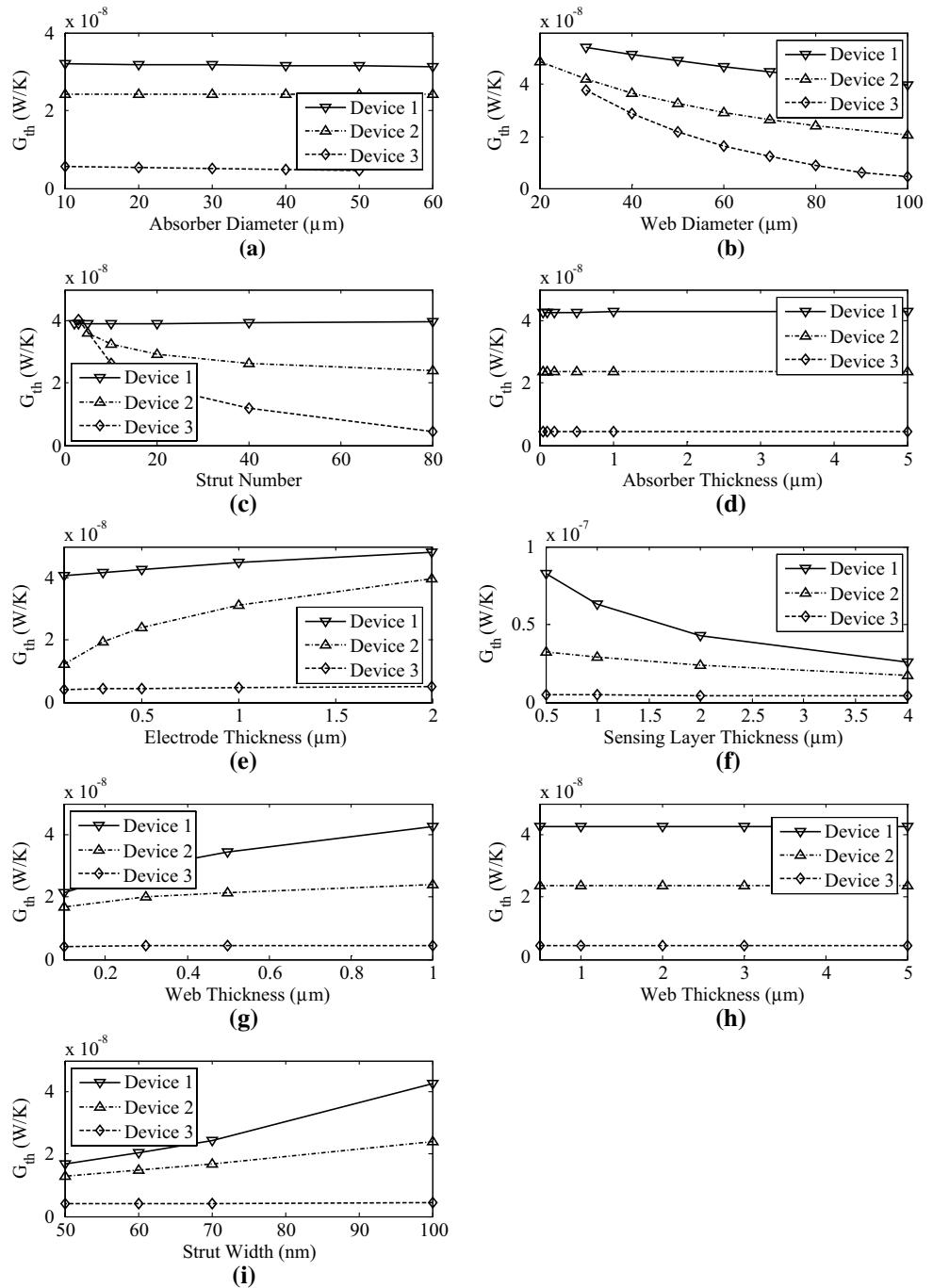
based on the web structure (see Fig. 3c) which exhibited the best performance among all three designs.

The dimension of the absorber had a little effect on thermal conductance as can be seen from Fig. 4a. From (7), it can be seen that the thermal conductance is a function of the ratio of absorber area to temperature rise which was found to be same for all the designs since absorber temperature was rising linearly with the area of the absorber. Hence, enough improvement was not found from this step.

Increasing the dimension of the spider web structure led to a lower thermal conductance. For all three designs, this modification was found to be advantageous as shown in Fig. 4b. A larger web structure had a longer path length which caused lower thermal conductance. However, an increase in the web structure size means a detector with more thermal mass and bigger size. So it put a limit on this step.

We found that the number of struts has a paramount effect on thermal conductance as shown in Fig. 4c. For
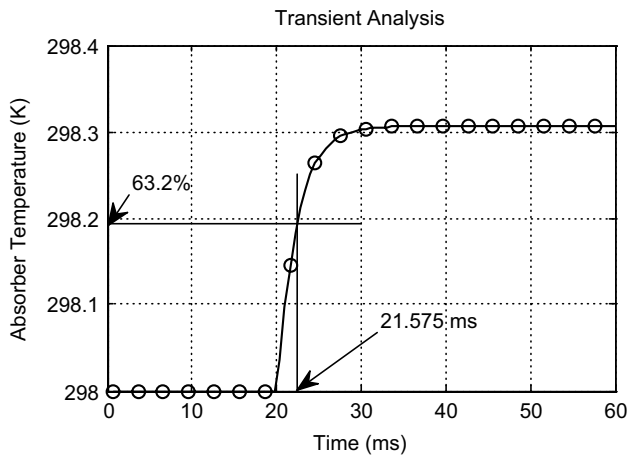
Fig. 5 Calculated heat transient analysis of the detector

device 2 and device 3, addition of struts provided longer thermal path length and hence reduced thermal conductance. However, more struts in the case of device 1 added more parallel paths for heat conduction and so it slightly increased the thermal conductance.

Absorber thickness did not demonstrate much effect on thermal conductance as revealed in Fig. 4d. That's because the thermal path due to the absorber thickness was negligible as compared to the total path length.

In the study of the effect of electrode thickness on thermal conductance (see Fig. 4e), it was found that device 1 and 2 showed some effects. This is because in device 1 and 2 the electrodes were directly responsible for heat conduction. Smaller thickness led to smaller cross-sectional area which provided a higher thermal resistance for conductive heat to transfer. However, for device 3 the meandered electrodes were conducting little heat along with the supporting structure and therefore did not show considerable change in thermal conductance.

A thicker sensing layer provides longer thermal path which helps in temperature rise. However, increase in thermal mass tends to increase thermal conductance. So, there was a race between these two factors and lower thermal conductance was found with increasing sensing layer thickness as demonstrated in Fig. 4f.

Because of lower thermal resistance due to larger cross-sectional area of thicker web structure, all devices showed increasing thermal conductance with increase in thickness of web structure as shown in Fig. 4g.

Not much effect of web support thickness was found on thermal conductance for any device as shown in Fig. 4h. This effect needs to be further investigated.

Study of strut width showed that decreased width can provide lower thermal conductance (see Fig. 4i). Struts with smaller width have smaller cross-sectional area and thus provide higher thermal resistance. Thus lower thermal conduction was obtained.

For the final design, the absorber diameter was 50 μm corresponding to the diameter of the spider web of 200 μm. Total 80 struts of 100 nm widths were used in the design. The thicknesses of the web structure, web support, electrodes, sensing layer and absorber of the optimized structure were 2, 1, 0.5, 2 and 0.2 μm respectively. The value of the thermal conductance of device 1 was found to be 3.98×10^{-8} W/K. Device 2 (see Fig. 3b) had a longer thermal path than the first one and the thermal conductance of this device was found to be 2.41×10^{-8} W/K. A detectivity of 1.15×10^{10} cm $Hz^{1/2}$/W was obtained (Balasubramaniyam 2010) by reducing the thermal conductance between the sensing layer and the substrate or the heat sink in the third design (see Fig. 3c). The thermal conductance between the sensor and the substrate using the third design was found to be as low as 4.57×10^{-9} W/K which is lower than the current reported values (Mahmood 2006, Balasubramaniyam 2010). The results are shown in Table 2. For each design the mechanical stability was tested and the maximum Von Mises stress was found to be much less than the yield strength of the materials.

The theoretical transient analysis for thermal behavior of the device was performed on the device and shown in Fig. 5. The thermal capacitance C_{th} was calculated from,

$$C_{th} = G_{th}\tau_{th} \tag{9}$$

where, τ_{th} is the response time found as the time interval for the absorber temperature to change from initial value to 63.2 % of the final value from Fig. 5. The thermal capacitance of the structure was found to be 7.198×10^{-12} J/K. This small value of thermal capacitance allows rise in temperature in the sensor with small amount of energy. It also helps in lower thermal conductance as can be seen in (7) and thereby improves the performance of the detector.

The theoretical transient analysis for electrical response of the pyroelectric detector was performed and shown in Fig. 6. The resistance of the R–C circuit is usually very high and so it was assumed to be 100 GΩ. The capacitance was calculated using (10).

$$C = \frac{\varepsilon A}{d} \tag{10}$$

The area of the capacitor (A) and permittivity (ε) was calculated to be 12×10^{-8} cm^2 and 1.532×10^{-11} F/cm respectively (Pontes et al. 2001). Electrical time constant was found as the time interval for the capacitor voltage to reach 63.2 % of the final value and found to be 0.908 ms.

The lower and upper cut off frequencies were calculated using (11) and (12) and found to be 100 and 175 Hz respectively.
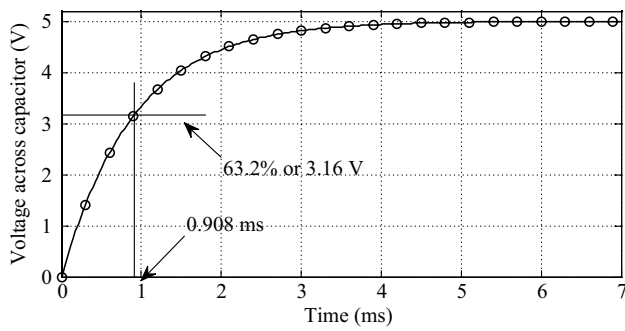
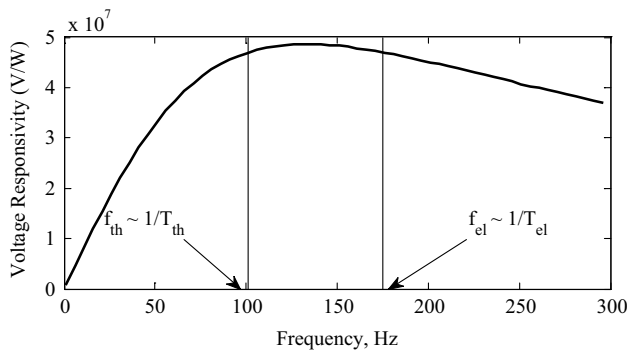**Fig. 6** Calculated electrical transient analysis of the detector

Fig. 7 Calculated voltage responsivity variation with frequency

$$f_{th} = \frac{1}{2\pi\,\tau_{th}} \tag{11}$$

$$f_{el} = \frac{1}{2\pi\,\tau_{el}} \tag{12}$$

The plot of voltage responsivity, R_v vs frequency, f is shown in Fig. 7. Pyroelectric coefficient used for the calculations was 46×10^{-9} C/cm²K (Mahmood 2006). There were three frequency regions. The first one was for $f < f_{th}$, where R_v increased linearly with f. For $f_{th} < f < f_{el}$, R_v remained almost constant and therefore this was the range of device operation. For $f > f_{el}$, R_v fell off linearly with f. The highest responsivity obtained was ~5×10^7 V/W.

The calculated values of Johnson and radiation noise at different frequencies are shown in Fig. 8. Johnson noise yielded the largest contribution and was decreasing with increasing value off.

The theoretical variations of noise equivalent power (NEP) and detectivity (D*) with respect to f is shown in Figs. 9 and 10 respectively. The detectivity of the detector was obtained in the order of 10^{10} cm $\sqrt{\text{Hz}}$/W. The detectivity was almost constant in the frequency range 100–175 Hz. High detectivity value was obtained from low value of NEP.
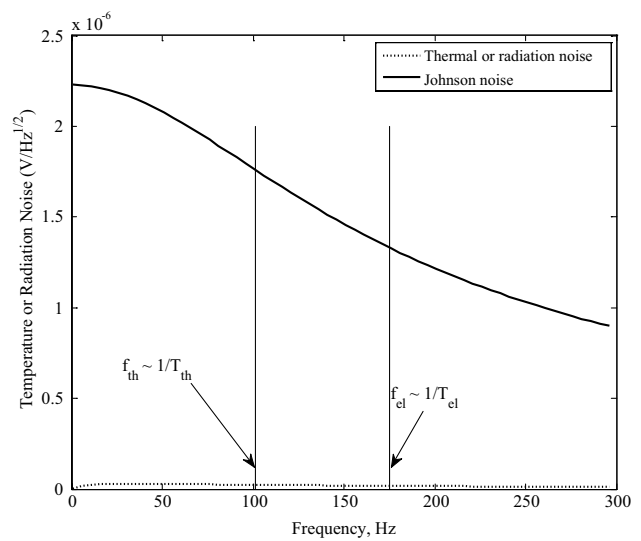

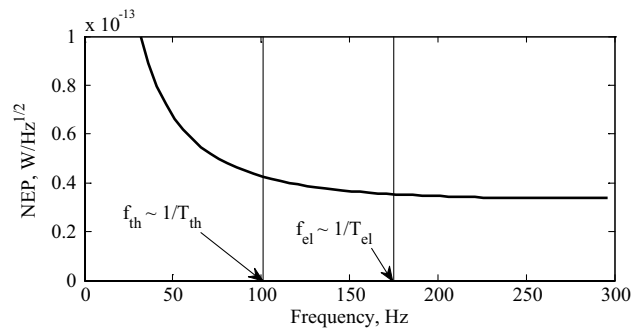**Fig. 8** Calculated variation of dominant noise sources with frequency

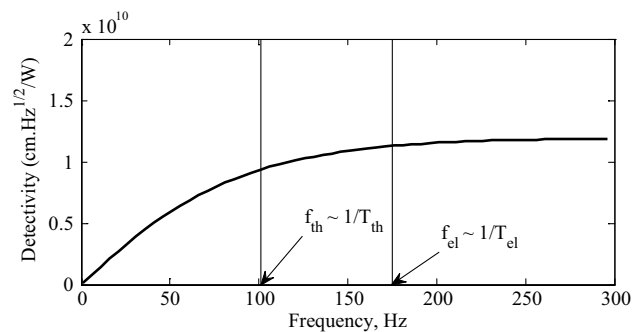**Fig. 9** Calculated variation of NEP with frequency

Fig. 10 Calculated variation of detectivity with frequency

4 Conclusions

Pyroelectric detector with nanometer size spider web was designed by using Intellisuite™ Engineering design software. The lowest thermal conductance between the sensor

and the substrate was obtained as low as 4.57×10^{-9} W/K compared to the radiative thermal conductance of 3.69×10^{-7} W/K (James and Lord 1992) from the simulation result. The low thermal conductivity obtained here by FEM, will yield a high sensitivity detector. The device can now be fabricated by using the designs proposed here. In the future increase of strut number can ensure even lower thermal conductance without increasing the device dimension. The major advantage of this type of thermal device is that it does not need external cooling, which improves the efficiency of the detector by a great factor. The designs will help to reduce the strut dimension from μm size strut to nm.

References

Balasubramaniyam A (2010) High detectivity pyroelectric infrared sensor. MS dissertation, The University of Texas at Arlington, Arlington, TX

Chang CC, Lai YC (2007) The fabrication and characterization of (Pb,Ca)TiO3 pyroelectric thin films with different Ca contents. J Appl Phys 101:104106

Chopra S, Sharma S, Goel TC, Mendiratta RG (2004) Ca substituted PbTiO3 thin films for infrared detectors. J Electroceram 13:155–158

Flannery RE, Milelr JE (1992) Status of uncooled infrared imagers. SPIE 1689:379–395

Gildemeister JM, Lee AT, Richards PL (2007) A fully lithographed voltage-baised superconducting spiderweb bolometer. Appl Phys Lett 101:104106

Glassbrenner CJ, Slack GA (1964) Thermal Conductivity of Silicon and Germanium from 3° K to the Melting Point. Phys Rev Lett 123:1058–1069

http://memsnet.org/material/. Accessed 1 Nov 2012

James AM, Lord MP (1992) Macmillan's Chemical and Physical Data. Macmillan, London

Kallaeva SN, Gadzhieva GG, Kamilova IK, Omarova ZM, Sadykovb SA, Reznichenko LA (2006) Thermal properties of PZT-based ferroelectric ceramics. Phys Solid State 48(6):1169–1170

Kao KC (2004) Electric Polarization and Relaxation. In: Dielectric phenomena in solids. Elsevier Academic Press, San Diego

Kiewiet FB, Brujn MP, Hoevers HFC, Bento AC, Mels WA, de Korte PAJ (1999) Fabrication and characterization of infrared and sub-mm spiderweb bolometers with low-Tc superconducting transition edge thermometers. IEEE Trans Appl Supercond 9:3862–3865

Kruse PW (1997) Chapter 2 principles of uncooled infrared focal plane arrays. Semicond Semimet 47:17–42

Mahmood A (2006) Device level vacuum packaged microbolometers on flexible substrates. PhD Dissertation, The University of Texas at Arlington, Arlington

Mehta VR, Shet S, Ravindra NM, Fiory AT, Lepselter MP (2005) Silicon-Integrated Uncooled Infrared Detectors: Perspectives on Thin Films and Microstructures. Electron Mater 34(5):484–490

Niklaus F, Vieider C, Jakobsen H (2007) MEMS-based uncooled infrared bolometer arrays: a review. SPIE 6836. doi:10.1117/12.755128

Parker TW, Marshall CA, Kohin M, Murphy R (1996) Uncooled infrared sensors for surveillance and law enforcement applications. SPIE 2935:182–187

Pontes DS, Leite ER, Pontes FM, Longo E, Varela JA (2001) Microstructural, dielectric and ferroelectric properties of calcium-modified lead titanate thin films derived by chemical processes. J Eur Ceram Soc 21:1107–1114

Qian J, Pantea C, Zhang J, Daeman LL, Zhao Y, Tang M, Uchida T, Wang Y (2005) Yield strength of a-Silicon nitride at high pressure and temperature. J Am Ceram Soc 88:903–906

Rajendra Kumara RT, Karunagarana B, Mangalaraja D, Narayandassa SK, Manoravib P, Joseph M, Gopal V (2003) Pulsed laser deposited vanadium oxide thin films for uncooled infrared detectors. Sens Actuators 107(1):62–67

Rogalski A (2003) Infrared detectors: status and trends. Quantum Eletron 27(2–3):59–210

Rossetti GA Jr, Maffei N, Physics J (2005) Specific heat study and Landau analysis of the phase transition in PbTiO3 single crystals. J Phys Condensed Matter 17:3953–3963

Seifert A, Muralt P, Setter N (1998) High figure-of-merit porous Pb1−xCaxTiO3 thin films for pyroelectric applications. Appl Phys Lett 72:2409